

THREE-MINUTE OSCILLATIONS ABOVE SUNSPOT UMBRA OBSERVED WITH THE *SOLAR DYNAMICS OBSERVATORY*/ATMOSPHERIC IMAGING ASSEMBLY AND NOBEYAMA RADIOHELIOGRAPH

V. E. REZNIKOVA¹, K. SHIBASAKI¹, R. A. SYCH^{2,3}, AND V. M. NAKARIAKOV^{4,5}

¹ Nobeyama Solar Radio Observatory/NAOJ, Nagano 384-1305, Japan; reznik@nro.nao.ac.jp

² Key Laboratory of Solar Activity, NAOC, Beijing 100012, China

³ Institute of Solar-Terrestrial Physics, P.O. Box 4026, Irkutsk, Russia

⁴ Physics Department, University of Warwick, Coventry CV4 7AL, UK

⁵ Central Astronomical Observatory at Pulkovo of the Russian Academy of Sciences, 196140 St. Petersburg, Russia

Received 2011 September 6; accepted 2011 November 24; published 2012 January 31

ABSTRACT

Three-minute oscillations over a sunspot's umbra in AR 11131 were observed simultaneously in UV/EUV emission by the *Solar Dynamics Observatory* (*SDO*)/Atmospheric Imaging Assembly (AIA) and in radio emission by the Nobeyama Radioheliograph (NoRH). We use 24 hr series of *SDO* and 8 hr series of NoRH observations to study spectral, spatial, and temporal variations of pulsations in the 5–9 mHz frequency range at different layers of the solar atmosphere. High spatial and temporal resolution of *SDO*/AIA in combination with long-duration observations allowed us to trace the variations of the cutoff frequency and spectrum of oscillations across the umbra. We found that higher frequency oscillations are more pronounced closer to the umbra's center, while the lower frequencies concentrate on the peripheral parts. We interpreted this discovery as a manifestation of variation of the magnetic field inclination across the umbra at the level of temperature minimum. Possible implications of this interpretation for the diagnostics of sunspot atmospheres are discussed.

Key words: Sun: oscillations – Sun: radio radiation – sunspots – Sun: UV radiation – waves

Online-only material: color figures

1. INTRODUCTION

Despite the fact that three-minute sunspot oscillations have been observed for many decades and enormous theoretical progress has been made in understanding this phenomenon (for reviews see Bogdan & Judge 2006; Thomas & Weiss 2008; Khomenko 2009), there are still many questions concerning sunspot wave physics. It is generally accepted that they are slow magnetoacoustic waves moving with the local sound speed along magnetic field lines from the photosphere through the chromosphere into the corona. However, it is still unclear how high in the corona they can propagate. What determines their properties in the corona? What is the spatial variation of the cutoff frequency across the umbra? Are they directly linked with the propagating longitudinal waves ubiquitously observed in the EUV fans of coronal active regions (ARs; for recent reviews, see, e.g., De Moortel 2009; Verwichte et al. 2010)? What is the nature of the recently revealed relationship of the three-minute oscillations and similar periodicities in flaring energy releases (Sych et al. 2009)? Understanding these issues provides an opportunity for a plasma diagnostic at different layers of the solar atmosphere since these waves convey the information about the properties of their formation and propagation mediums. Thus, Shibasaki (2001) proposed that umbral oscillations seen in microwaves can be used as a diagnostic of the temperature-minimum region. Further, Solanki (2003) pointed out that observations with higher spatial resolution are needed to isolate the umbra and to improve the diagnostics.

Spatial distribution of three-minute oscillation frequency and power across a sunspot at different heights has been intensively studied with the use of data obtained with ground-based and space-borne instruments (e.g., on board *Solar and Heliospheric Observatory* (*SOHO*), *Transition Region and Coronal Explorer* (*TRACE*), and *Hinode*). In particular, observations made with the Michelson Doppler Imager (MDI) showed that

at the photosphere the oscillation power is enhanced in the Doppler velocity and line-depth signals, but not in the continuum intensity (Jain & Haber 2002). Enhancement of the spectral power was found in regions of reasonably strong magnetic field, but regions of strongest fields, in the center of the sunspot, showed evident suppression of power. Observations in H α demonstrated that standing oscillations with frequencies around 6.5 mHz were dominant in the umbral and inner penumbral regions, together with the presence of running penumbral waves in the band of 3 mHz. However, these waves were not detected at the photospheric heights (Christopoulou et al. 2000, 2001). It was suggested that both three-minute umbral oscillations and five-minute running penumbral waves were in fact different manifestations of the same wave, generated in the photosphere and propagating along different magnetic field lines with a different inclination angle (van der Voort et al. 2003; Bloomfield et al. 2007). Christopoulou et al. (2003) demonstrated that oscillations with different frequencies in the three-minute band were localized within different parts of the umbral chromosphere. Then Tziotziou et al. (2006) found that in the chromosphere, the frequency of three-minute oscillations decreases from the umbra outward, with the abrupt change at the umbra–penumbra boundary. A small “node” at the center of the umbra, where the oscillations with frequencies above 4 mHz were suppressed, was reported by Nagashima et al. (2007). A similar effect of “calmest umbral position” was found in the Doppler velocity maps in Ca II λ 8542 by Tziotziou et al. (2007). The nature of this “black spot” in the spatial distribution of the chromospheric three-minute oscillations remains unrevealed.

In the transition region the three-minute oscillations are reported to fill in all the sunspot umbra. In the corona they concentrate on smaller regions that coincide with the endpoints of bright coronal loops (Brynildsen et al. 2000, 2002, 2004). De Moortel et al. (2002) used *TRACE* observations of EUV

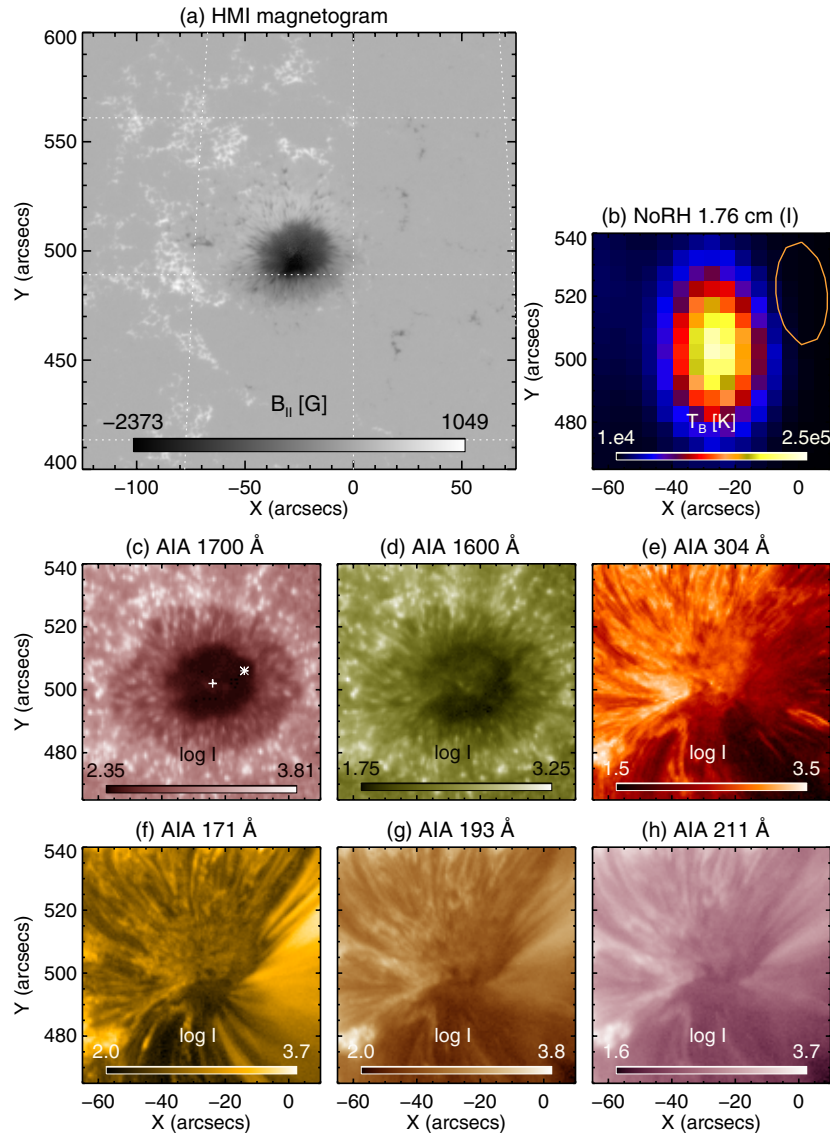


Figure 1. (a) *SDO*/HMI magnetogram of the sunspot region in NOAA AR 11131 and images of the sunspot taken (b) by NoRH and (c–h) by *SDO*/AIA on 2010 December 8 at 04:00 UT. Orange ellipse at top right of plot (b) indicates the half-maximum NoRH beam size. White cross and asterisk on plot (c) indicate two pixels inside the umbra for later reference.

(A color version of this figure is available in the online journal.)

intensity waves in 38 coronal loops and found that in the loops situated above sunspots the waves have periods of about 3 minutes. This suggests that the underlying oscillations can propagate through the transition region into the corona.

Hence, it is still not clear how the oscillation power and frequency in the three-minute band are distributed within the umbra of the sunspot at different altitudes. This knowledge is important for revealing the nature of three-minute oscillations and for a diagnostic of the solar atmosphere above sunspots.

The data from the Atmospheric Imaging Assembly (AIA; Title et al. 2006) on the *Solar Dynamics Observatory* (*SDO*; Schwer et al. 2002), with their high resolution ($0.6 \text{ arcsec pixel}^{-1}$) and high cadence (up to 12 s), offer a new opportunity for such a study. The instrument observes solar plasma from photospheric to coronal temperatures, taking full-disk images in a variety of EUV, UV, and visible light wavelength bands. The other advantage of *SDO* data is 24 hr continuous observations. Three-minute oscillations have very high quality; they can be observed for many days. Therefore, long-duration

observations allow us to study this phenomenon with very high spectral resolution, which has not been done before.

In this paper, we analyze simultaneous observations of the sunspot-associated oscillations by two instruments, AIA and the Nobeyama Radioheliograph (NoRH), in order to obtain information on spectral, spatial, and temporal structures of oscillations above the same sunspot. We restrict our analysis to the frequency range 5–9 mHz and horizontal extent to the umbral area.

2. OBSERVATIONS

AR 11131 was available for observations in the northern hemisphere near 30° latitude and crossed the central meridian on 2010 December 8. We selected this date for our analysis. Figure 1(a) presents the line-of-sight magnetogram of the sunspot region from the Helioseismic and Magnetic Imager (HMI) on *SDO*. AR 11131 consisted of a well-developed sunspot of southern polarity with the magnetic field strong

enough, $B = -2300$ G, to produce the significant and highly polarized emission at 17 GHz ($\lambda = 1.76$ cm). The sunspot was surrounded by a number of small magnetic fragments of northern polarity.

The emission mechanism of radio sources associated with sunspots is known to be gyroresonance emission (e.g., Zheleznyakov 1962). At 17 GHz, the third harmonic layer is the most probable emission region, corresponding to a 2000 G isogauss layer (Shibasaki et al. 1994).

The radio map of the sunspot obtained from NoRH is shown in Figure 1(b). Color indicates brightness temperature at 1.76 cm (Stokes I). NoRH measures both the right circular polarization and left circular polarization. Using these measurements, we synthesized a set of NoRH images in the I and V Stokes parameters with a time interval of 10 s. The NoRH beam width (FWHM) is indicated by the orange ellipse at the topright. Owing to low elevation of the Sun during the wintertime, the beam size was roughly $17'' \times 30''$, comparable with the radio source, and therefore determined an elliptical shape of the latter.

In Figures 1(c)–(h), we show the intensity images of the sunspot in a sequence of increasing temperatures from six AIA bandpasses: 1700, 1600, 304, 171, 193, and 211 Å. The spatial resolution of data is 0.6 arcsec pixel $^{-1}$.

AIA observes a UV continuum in the 1700 Å bandpass with the characteristic formation temperature of about 5000 K. This bandpass corresponds to the lowest formation layer located close to, but still above the temperature-minimum region. According to the sunspot atmospheric model by Maltby et al. (1986), the temperature-minimum region is located at about 500 km above $\tau_{500} = 1$, corresponding to the upper photosphere/lower chromosphere. The AIA 1600 Å bandpass has a broad response to temperatures ranging from the temperature minimum to chromospheric line C IV emissions ($(4\text{--}10) \times 10^3$ K) in ARs, but the dominant contributor is the UV continuum above the region of temperature minimum. The 304 Å channel is dominated by the two He II lines with average formation temperature $T = 5 \times 10^4$ K, corresponding to the transition region. EUV light from the Fe IX emission line in the 171 Å bandpass comes primarily from the upper transition region/quiet corona material with average formation temperature $T = 6.5 \times 10^5$ K. The 193 Å channel is expected to be dominated by the Fe XII line (average $T = 1.5 \times 10^6$ K), and the 211 Å channel is expected to observe the Fe XIV line ($T = 2 \times 10^6$ K) for AR observations (O'Dwyer et al. 2010).

We did not use the other SDO/AIA bandpasses for the following reasons: visible light continuum observations at 4500 Å are available only with 3600 s time cadence, and observations in coronal channels 94 and 131 Å did not have sufficient quality for this sunspot.

3. DATA ANALYSIS

3.1. Temporal Variations of UV/EUV and Microwave Emission

It is known that changes in the UV/EUV emission with time must be due to changes in the temperature and density in the emission-forming region. Plasma temperature and density variations, in turn, are thought to be evidence of some dynamical processes, e.g., a compressible wave passage through the corresponding region.

Different interpretations for the radio brightness oscillation were proposed, for example, as being caused by the variations in magnetic field strength (Gelfreikh et al. 1999). Shibasaki (2001), however, showed that they can be explained consistently with

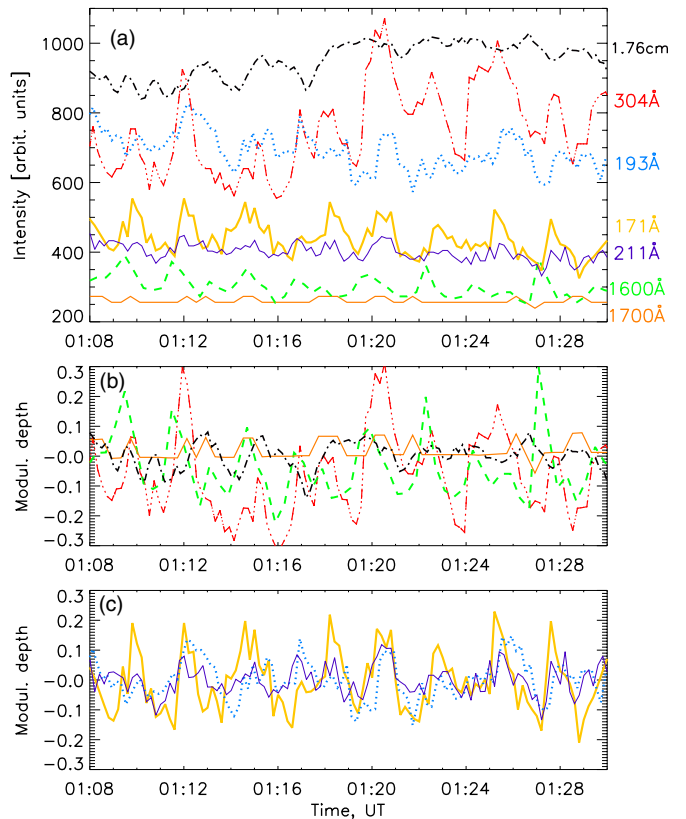


Figure 2. (a) The time profiles of intensity above the center of the umbra from six AIA bandpasses and $T_{B\max}$ at 1.76 cm of 22 minute duration. Emission modulation depth at (b) 1700 Å (solid), 1600 Å (dash), 304 Å (dash-dot-dotted), and 1.76 cm (dash-dotted) and (c) 171 Å (thick), 193 Å (dots), and 211 Å (thin). For the color version of the figure, different wavelengths are shown by colors, corresponding to the key to the right.

(A color version of this figure is available in the online journal.)

the EUV observation in terms of the density and temperature fluctuations due to upward-traveling acoustic waves through the third harmonic gyroresonance layer (2000 G for observations at 1.76 cm).

To study temporal variations of UV/EUV emission above the center of the umbra, where the magnetic field is presumably vertical, we analyzed de-rotated 24 hr series of intensity obtained from 1 pixel, corresponding to the umbra's center and shown by the white cross on the 1700 Å image of Figure 1(c). The neighboring pixels show a very similar time variability; hence, the data are not affected by the possible variation in pointing. For microwave emission we picked up the value of the maximum brightness temperature, $T_{B\max}$, located at the center of the elliptical source and therefore corresponding to the sunspot umbra center for every synthesized map.

Figure 2(a) shows time profiles, $I(t)$, of the UV/EUV intensity (in arbitrary units) and microwave peak brightness temperature (in K) of 22 minute duration for clarity. A 1600 Å intensity is multiplied by a factor of three and NoRH 1.76 cm brightness temperature by a factor of 4×10^{-3} . The time cadence is 24 s for 1700 and 1600 Å, 10 s for 1.76 cm, and 12 s for other channels. The well-pronounced variations of the emission intensity, with periods of about 2–3 minutes, are clearly seen in all channels.

The time profiles of the modulation depth are shown in Figure 2(b) for 1700 Å, 1600 Å, 304 Å, and 1.76 cm and in Figure 2(c) for 171, 193, and 211 Å using the same colors as

in Figure 2(a). This quantity is calculated as

$$\Delta I/I = [I(t) - I_0]/I_0, \quad (1)$$

where $I(t)$ is the time series of intensity of UV/EUV or microwave brightness temperature. The slowly varying mean signal I_0 is obtained by smoothing the signal $I(t)$ over an interval of 14 minutes. The highest modulation depth is found for 304 Å emission, 20% on the average, and it decreases down to the photosphere, 10% for 1600 Å and 8% for 1700 Å, and up to the corona with height, 18% for 171 Å, 12% for 193 Å, and 8% for 211 Å.

Modulation depth 5% is found for microwave brightness variation. It corresponds to the change in brightness temperature by $\Delta T_B \approx 1.2 \times 10^4$ K. These values agree with previous results showing 1%–5% of T_B variation.

The general trend of the height change in modulation depth of UV/EUV emission also agrees with results of previous studies, which have shown that the oscillation amplitude peaks at transition region temperatures (e.g., O’Shea et al. 2002; Marsh & Walsh 2006). However, it is rather surprising to find intensity variations with such a high amplitude in coronal channels. Previous studies showed umbral oscillations, observed with *TRACE* 171 and 195 Å, with much smaller amplitudes (3%–8%) usually guided along the EUV fans of the limited transverse size. One possibility is the presence in the coronal EUV channels of AIA of the emission generated at much lower temperature and hence heights. Brynildsen et al. (2004) estimated the contributions from the transition region lines to the *TRACE* 171 and 195 Å channel intensity. They found an average value of these contributions equal to 17% and finally concluded that the significant part of the oscillations in the *TRACE* 171 and 195 Å channels must indeed occur in the corona. O’Dwyer et al. (2010) performed a similar examination for AIA and found that the dominant contribution to three EUV coronal channels under study from the AR plasma comes from the expected ion line formed at the hot, coronal temperatures.

3.2. Cross-correlation Analysis

The other indirect indicator of the brightness fluctuation origin in each AIA channel can be time shifts between corresponding signals. If the pulsations originate from the same layer of the solar atmosphere, we may expect an in-phase behavior for intensity variations.

Cross-correlation coefficients as a function of the lag for each analyzed wavelength with respect to 304 Å intensity variation are shown in Figure 3(a), and corresponding delays in Figure 3(b). We used temporal interpolation of the 304 Å time series to match other channel observing times. The precision limit of the obtained delays is estimated by $\sigma = k \times \sigma_s$, where $\sigma_s = \sqrt{\Delta t^2}/12$ is the standard deviation of the sampling error for the uniform time resolution Δt and $k = 2$ for 95% confidence from the Student’s t -distribution. These uncertainties $\pm \sigma$ are shown by error bars in Figure 3(b).

Time delays increase with the expected formation height of different channels, except the 211 Å channel. Equal delay for 171 and 211 Å ($12 \text{ s} \pm 7 \text{ s}$) supposes that possibly the 211 Å intensity has a contribution of cooler temperature lines than expected, or the cooler and hotter plasma structures simply coexist in the corona at the same height. At the same time, increasing delays found for other wavelengths suggest that observed intensity variations in different channels originate from progressively higher altitudes and result from waves

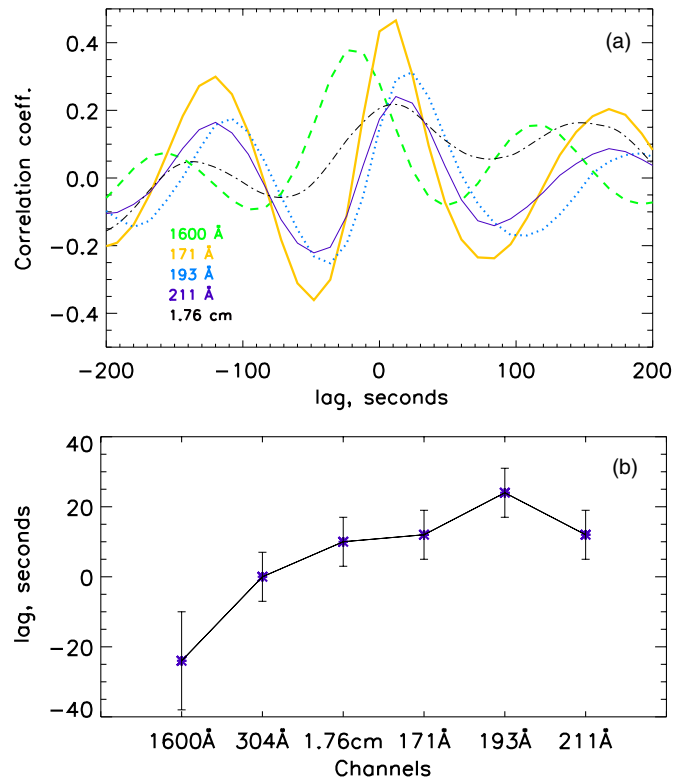


Figure 3. (a) Cross-correlation coefficients of long time series of pulsations above the umbra’s center of each analyzed wavelength with respect to 304 Å as a function of the lag. The same colors and line types as in Figure 2 are used to indicate different wavelengths. (b) Time lags obtained from cross correlation for each wavelength with the corresponding uncertainties shown by error bars. (A color version of this figure is available in the online journal.)

propagating upward along magnetic field lines. The cross-correlation coefficient for the 1700 Å bandpass is poor, probably as a result of very weak emission variation inside the umbra region and nonuniform temporal resolution of downloaded data, and is not shown here.

If we estimate the expected height separation ΔH between the two consecutive AIA wavelengths based on the mean formation temperatures mentioned in Section 2, we can use obtained delays to make rough estimates of the average velocity of wave propagation between the two heights. Assuming 1600 Å formation height around temperature minimum (about 500 km) and 304 Å in the transition region (about 2200 km), $\Delta H_1 \approx 1700$ km gives vertical velocity $v_1 \approx 70 \text{ km s}^{-1}$. This value exceeds the speed of sound in the chromosphere, which lies between 10 and 30 km s^{-1} . However, Abramov-Maximov et al. (2011) found a close value of speed (60 km s^{-1}) based on cross-correlation between optical and radio oscillations.

The height separation $\Delta H_2 \approx 1000$ km between the heights of the 304 and 171 Å emission layers gives velocity $v_2 \approx 83 \text{ km s}^{-1}$. This value corresponds to the calculated sound speed with $T = 2 \times 10^5$ K, which is an average temperature between the two formation layers.

It is rather difficult to define the height of the 193 Å emission formation over the sunspot umbra. Bearing in mind the speed of sound (130 km s^{-1}) calculated for the 171 Å emission formation temperature (6.5×10^5 K), the delay $12 \text{ s} \pm 7 \text{ s}$ between the 171 and 193 Å emissions gives the minimum value of $\Delta H_3 \geq 1500$ km. Therefore, the 193 Å emission above the umbra corresponds to the corona with $T \geq 1$ MK.

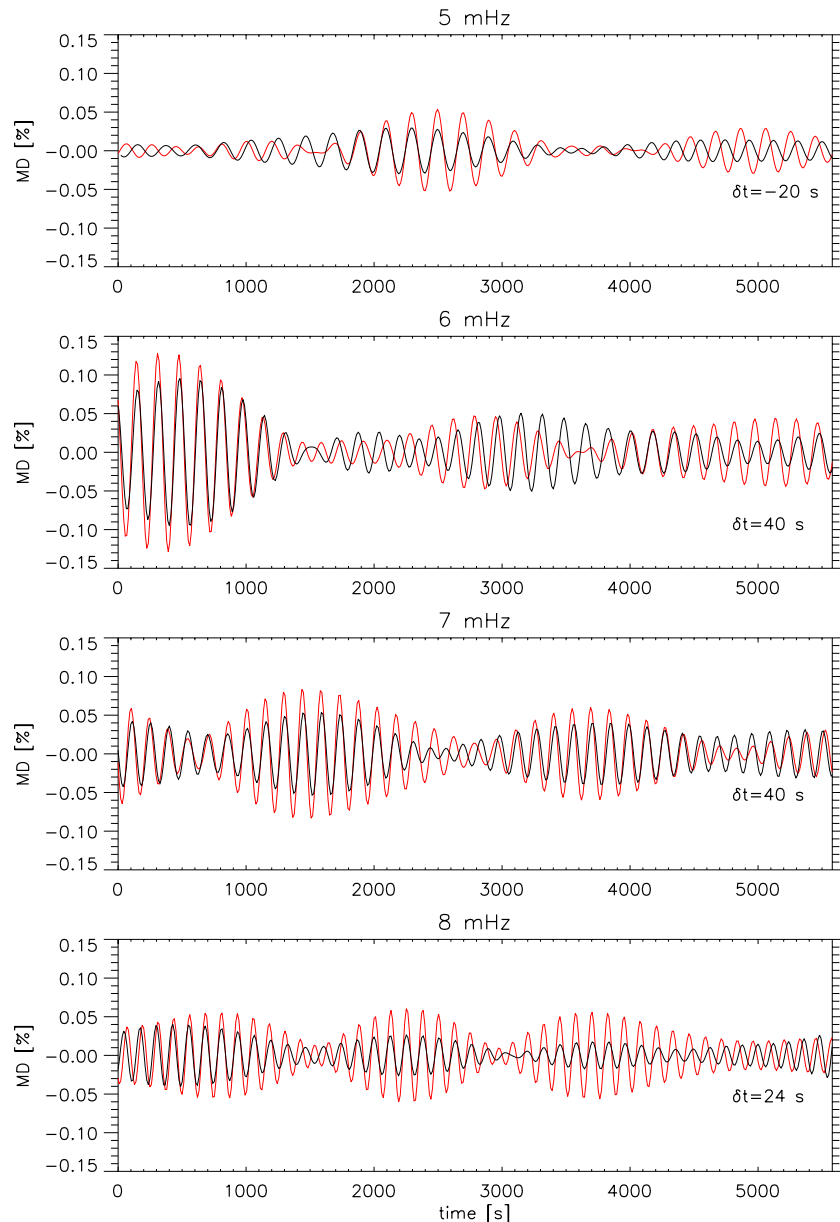


Figure 4. Emission modulation depth of signals at 304 Å (red) and 193 Å (black) from the center of the umbra filtered in narrow (1 mHz) frequency bands with the central frequencies at 5, 6, 7, and 8 mHz (± 0.5 mHz). Signals at two frequencies are overplotted with a time shift δt to match each other.

(A color version of this figure is available in the online journal.)

Cross-correlation analysis gives $10 \text{ s} \pm 7 \text{ s}$ of the time delay between the 304 Å and microwave signals, which means that the formation height of radio emission is between the AIA 304 and 171 Å bandpasses. Using $v_2 \approx 83 \text{ km s}^{-1}$ obtained for this height interval, we estimated the altitude of 1.76 cm emission generation, which is approximately 3000 km. The observed value of peak brightness temperature $T_{\text{Bmax}} = 2.5 \times 10^5 \text{ K}$ exactly corresponds to the estimated altitude.

We have to note that the time delays presented in Figure 3 are averaged over the frequencies and time. Further analysis reveals that these delays are frequency and time dependent. In Figure 4, we show the emission modulation depth of signals at 304 Å (red) and 193 Å (black) at the center of the umbra, shifted in time by δt to match each other. Signals are filtered in narrow (1 mHz) frequency bands with the central frequencies at 5, 6, 7, and 8 mHz (± 0.5 mHz). In this example, the 193 Å signal is delayed against the 304 Å signal by 40 s at 6 and 7 mHz and

by 24 s at 8 mHz. But at 5 mHz we found an inverse delay: the 304 Å signal is delayed against the 193 Å signal. Moreover, these phase delays are not only frequency dependent but also time dependent: though by varying the time shift δt we could adjust the phases of the signals in one wave train, the same phase shift did not do it in the other wave train. The phase shifts were found to vary strongly during the 24 hr observation. Often it was not easy to resolve the 2π uncertainty.

The fact of the frequency dependence of the delays between the signals measured at different heights agrees with previous empirical results obtained from the cross-correlation of photospheric and chromospheric velocity maps filtered in narrow bands (Centeno et al. 2006, 2009), as well as with the theoretical prediction that oscillation modes in a dispersive medium propagate with the phase velocity depending on the frequency. The time dependence is also consistent with the previous results, e.g., the frequency drifts in the three-minute band

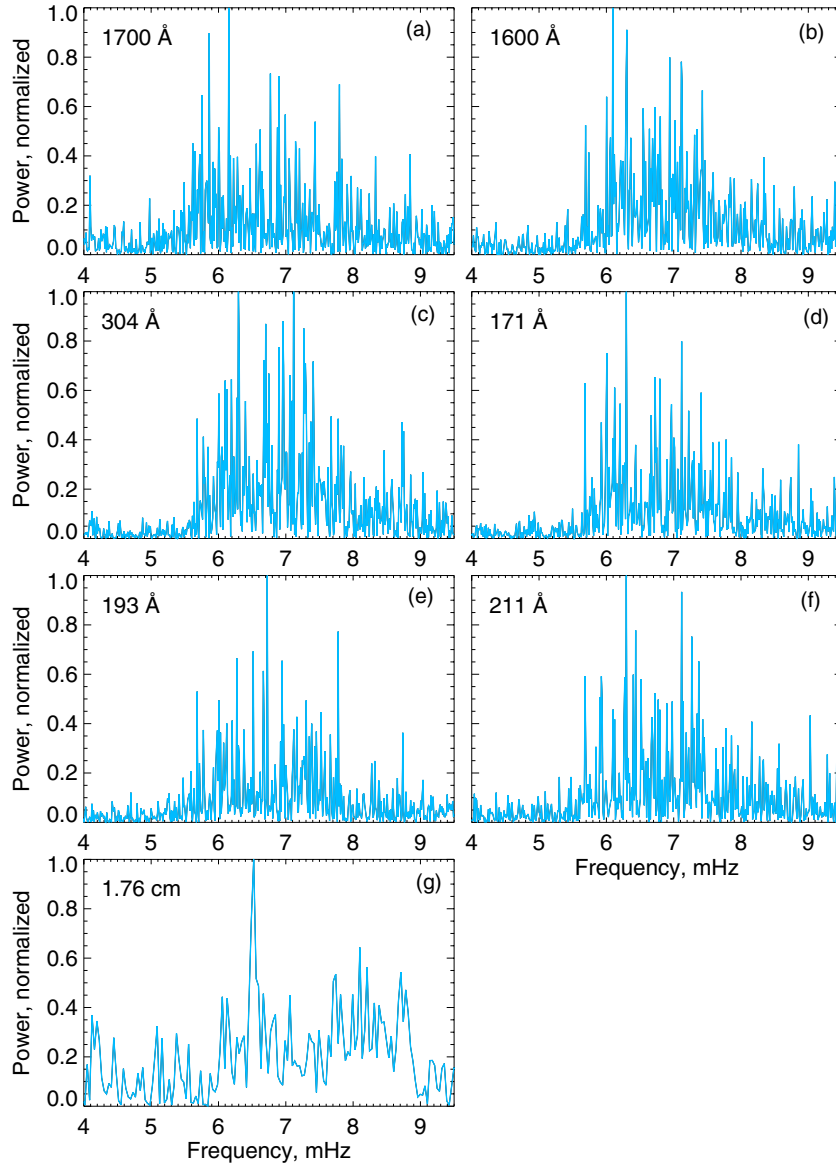


Figure 5. Fourier power spectra of the intensity variation above the center of the umbra for all analyzed wavelengths. (A color version of this figure is available in the online journal.)

(Christopoulou et al. 2003; Sych et al. 2011). Therefore, detailed analysis of the phase relations between the perturbations at different heights is of obvious interest. However, it is beyond the scope of this paper and will be addressed in a follow-up study.

3.3. Spectral Analysis

To study the spectral characteristics of intensity variation, we used the fast Fourier transform method. Because of long intervals of uniform data with high cadence, the spectral analysis was done with high-frequency resolution, $36 \mu\text{Hz}$ for NoRH and $12 \mu\text{Hz}$ for AIA. Such high spectral resolution in combination with the high spatial and temporal resolution of *SDO/AIA* allowed us to trace the variations of the spectrum of three-minute oscillations across the umbra. In particular, we were able to trace the so-called low cutoff frequency, which is defined here as the lowest frequency in the 4–9 mHz band for which the Fourier power is three times higher than the noise level.

Figure 5 represents the power spectra covering 24 hr of UV/EUV data and 7 hr 45 minutes of microwave data. The

power is normalized on its maximum in the 4–10 mHz band. The spectra are shown for the single pixel above the center of the umbra. Most of the spectra have dominant frequencies between 6 mHz (period 167 s) and 7 mHz (period 143 s). The high-frequency tail extends beyond 8 mHz. All UV/EUV spectra exhibit a sharp increase at 5.7 mHz (equivalent period 175 s), which can be considered as the lower cutoff frequency.

It is interesting to note that a similar value (5.8 mHz) was recently found for the maximum cutoff frequency at the axis of a model sunspot in the three-dimensional nonlinear MHD simulation with the driver located under the photosphere and emitting five-minute waves (Felipe et al. 2010).

The spectrum of the radio oscillation at 1.76 cm does not show a clear low cutoff. However, the microwave signal has a duration of less than three times that of the UV and EUV data and comes from a much larger area: the difference in the pixel size of AIA and NoRH maps is about 10 times. Nevertheless, similar to all AIA spectra, it has a maximum between 6 and 7 mHz and an increase in the power near 8.8 mHz.

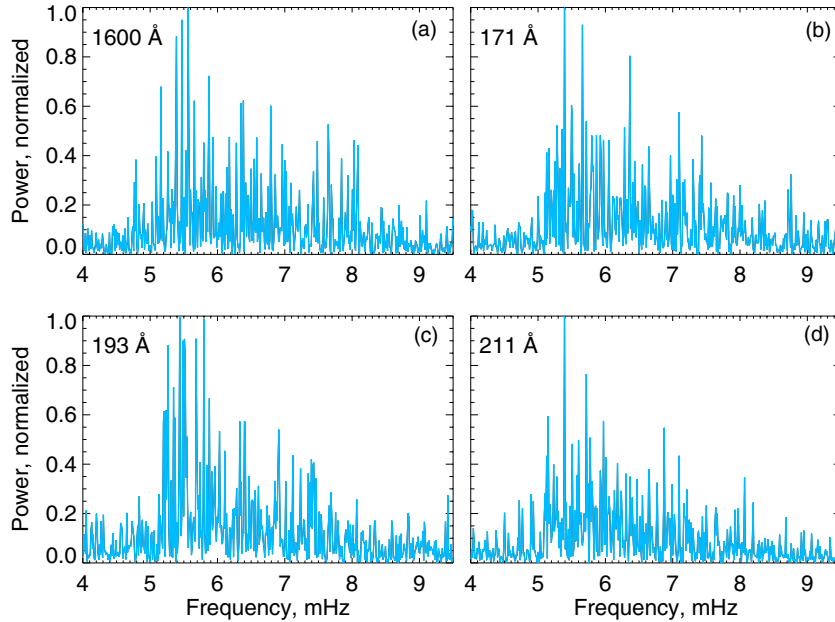


Figure 6. Fourier power spectra of the intensity variation near the umbra/penumbra border from four AIA bandpasses. (A color version of this figure is available in the online journal.)

In previous studies the value of the cutoff frequency was often defined as the highest frequency where the phase difference between two signals measured at different heights was zero (e.g., Centeno et al. 2006, 2009; Felipe et al. 2011). As we see from Figure 4, the phase difference between the 193 and 304 Å signals is positive in the 6–8 mHz band, while it is negative at 5 mHz. This confirms that the cutoff frequency is located between 5 and 6 mHz. However, the above-mentioned method allows one to determine the cutoff frequency averaged over the umbra, while we are interested in the spatial distribution of this value across the umbra.

Further analysis has shown that spectral characteristics of oscillations vary across the umbra. Figure 6 presents the spectra for pixels located farther from the center, near the umbra/penumbra border, which is shown by the white asterisk in Figure 1(c). It is clearly seen that the low-frequency cutoff dropped down to 5 mHz and the peak frequency moved down to 5.5 mHz as compared with the umbra’s center. The same tendency is found for all other AIA channels.

To trace the changes in the spectrum of oscillations for the entire sunspot region, we calculated the Fourier power spectra for every spatial pixel of the intensity maps. Figure 7 gives the spatial distribution of the Fourier power in four narrow ($\Delta f = 0.4$ mHz) frequency bands with the central frequencies at 5, 5.5, 6, and 7 mHz (± 0.2 mHz in each band). Individual power spectra from each spatial pixel have been normalized on its spectral maximum. Normalization was performed to aid in the comparison of spectral profiles between spatial regions that exhibit vastly different intensity amplitudes. Only pixels with power larger than three times the noise level are plotted in the power spectrum maps. The umbra–penumbra boundary as observed in the 1700 Å continuum is shown in every plot by the contour line, white in panels (a and b) and black in panels (c–f). The external penumbra border is also shown in the upper left plot of panel (a) for reference.

It is clearly seen from Figure 7(a) that the Fourier power in all four frequency bands is confined inside the umbra and avoids the penumbral region. In the 5 mHz band it also

avoids the central part of the umbra and forms a ring near the umbra/penumbra border. In the 5.5 mHz band this ring extends inside the umbra, becoming wider. We already saw in Figure 5 that oscillations at frequencies $f < 5.7$ mHz are absent in the center of the sunspot. Oscillations in the 6 and 7 mHz bands cover the whole umbra but are more pronounced in its central part. This tendency is seen through all the AIA bandpasses; see Figures 7(b)–(f). At the same time, the oscillating area slightly broadens with the height. The diameter of the oscillating circle is widened by about $\Delta d = 1''$ with each subsequent bandpass, expanding beyond the umbra boundary at 304 Å. In coronal channels 171–211 Å pulsations with high power outspread to the coronal fan structures. Higher frequencies, 8 and 9 mHz, exhibit even stronger concentration toward the center, but lower power (they are not shown here).

The peculiarities of the spatial distribution of three-minute oscillation frequency found here are consistent with previously obtained results, in particular, with the decrease in the peak frequency from the umbra outward, and with the abrupt change in the umbra–penumbra boundary in the chromosphere, reported by Tziotziou et al. (2006). Also, the existence of the region with the suppressed power of three-minute oscillations at the center of the umbra has been found by Jain & Haber (2002) in the photospheric Doppler velocity and line-depth data of *SOHO*/MDI, by Nagashima et al. (2007) at lower frequencies (5–5.5 mHz) using Solar Optical Telescope observations of low-chromospheric Ca II H line intensity, and by Tziotziou et al. (2007) in their Doppler velocity maps obtained at Ca II 8542 Å. Here, we show that such a region at 5–5.5 mHz exists also at the transition region and coronal heights and that its size is frequency dependent.

4. INTERPRETATION OF SPECTRAL CHARACTERISTICS

It is interesting to note that the spectral characteristics of three-minute oscillations, namely, the low cutoff frequency and its variation across the umbra, are similar through all the

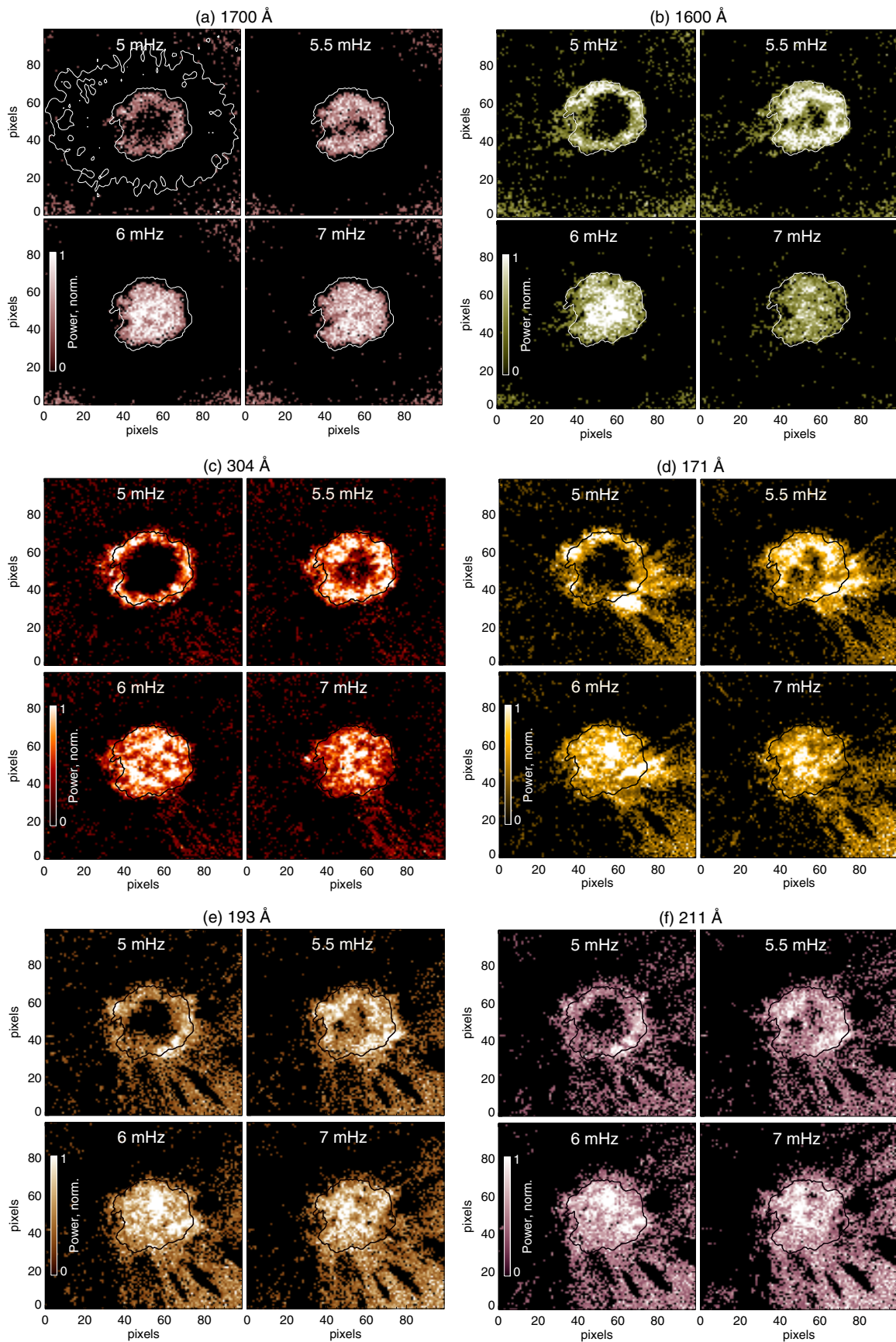


Figure 7. Spatial distribution of normalized Fourier power in four frequency bands with the central frequencies at 5, 5.5, 6, and 7 mHz (± 0.2 mHz in each band). Power grows with brightness. The umbra–penumbra boundary is shown by contour lines, white on panels (a) and (b) and black on panels (c–f).

(A color version of this figure is available in the online journal.)

temperature bandpasses. This finding suggests that the strong magnetic field of a sunspot works as a waveguide for the acoustic waves generated already at the photosphere level and eventually reaching a 1 MK corona.

To understand the spectral characteristics of three-minute oscillations above the umbra and the tendency of their spatial distribution, we start from the generally accepted idea that these oscillations are caused by magnetoacoustic gravity (MAG) waves, that is, the acoustic-like slow mode propagation along the magnetic field lines. It has long been known (since Lamb 1908) that, owing to the presence of gravitational field, compressible acoustic waves can propagate upward through the temperature minimum only at frequencies above the cutoff frequency:

$$f_c = \frac{g\gamma}{2\pi C_s}, \quad (2)$$

where g is the gravitational acceleration and

$$C_s = \sqrt{\gamma RT/\mu} \quad (3)$$

is the speed of sound, T is the temperature, γ is the ratio of specific heats, μ is the mean molecular weight, and R is the gas constant.

Further, Bel & Leroy (1977) showed that for MAG waves in the solar atmosphere the cutoff frequency will be affected by the magnetic field when it is not parallel to the gravitational field. They predicted that in regions of low- β plasma ($\beta \ll 1$), which is the case above the sunspot umbra, the effective gravity on a particular magnetic field line would be decreased by the cosine of the inclination angle θ of that field line with respect to the direction of gravity (the solar normal), which is

$$g = g_0 \times \cos \theta, \quad (4)$$

where $g_0 = 274 \text{ m s}^{-2}$. Therefore, the cutoff frequency

$$f_c \propto \cos \theta / \sqrt{T}. \quad (5)$$

Based on the above theoretical predictions, one may expect that the change of the observed cutoff frequency across the umbra may result from either the variation of temperature in the temperature-minimum layer, T_{\min} , becoming smaller in the center of the umbra or the magnetic field inclination angle θ becoming large enough near the umbra/penumbra border. The upper limit of f_c is determined by T_{\min} on the path of the MAG wave propagating along the vertical field line.

According to Figure 5, the value of the cutoff frequency in the center of the umbra, in exactly vertical field, is $f_c = 5.7 \text{ mHz}$. If, following Fleck & Schmitz (1991), we take $\mu = 1.3$ and $\gamma = 5/3$ for an ideal neutral gas, using Equation (2) we obtain $T_{\min} \approx 3800 \text{ K}$. The uncertainty of this estimate is mainly determined by the uncertainty of the mean molecular weight μ : change in μ by 0.1 gives a change in temperature of 300 K. Moreover, the mean molecular weight in turn depends on temperature.

Near the umbra's boundary we found $f_c = 5 \text{ mHz}$. Using proportionality (5) under the assumption of $T_{\min} = \text{const.}$ gives the inclination angle $\theta \approx 30^\circ$ at the peripheral parts of the umbra. This value is consistent with the results of previous studies of the radial variation of field inclination on the level of the temperature minimum (e.g., Figure 3 in McIntosh & Jefferies 2006).

On the other hand, it is reasonable to assume that the minimum temperature grows from the middle to the peripheral parts of the

umbra. Under the assumption of vertical field through the entire umbra, the observed value $f_c = 5 \text{ mHz}$ gives $T_{\min} \approx 4900 \text{ K}$. This value is too large even for the quiet-Sun atmosphere (Avrett & Loeser 2008). Therefore, we think that the temperature increase has a smaller effect on the wave frequency distribution across the umbra than the magnetic field inclination, though both effects modify the cutoff frequency in a similar way.

The gradual broadening of the area occupied by the oscillations with the height of the solar atmosphere agrees well with the above interpretation. Roughly speaking, those field lines inclined 30° to the solar normal must form a wider circle in the transition region than at the temperature-minimum level. An estimate using the simplifying assumption that the magnetic field remains linear between the two formation heights (there is no field curvature) gives $1''\text{--}2''$ of the circle expansion. This estimate agrees well with the observed value Δd shown in Section 3.3.

An observational demonstration of the acoustic cutoff frequency modification in the penumbra area using TRACE observations is presented by McIntosh & Jefferies (2006). Results obtained in this work can be considered as a demonstration of the same effect in the umbral area. Nevertheless, magnetic field extrapolation would be useful to confirm it.

The other possible explanation of ring-like frequency-spatial structure can be found in the frame of the chromospheric acoustic resonator model (Zhugzhda 2008; Botha et al. 2011). Indeed, as the angle of the guiding magnetic field from vertical increases, the size of the resonator grows and hence the resonant frequency decreases.

5. CONCLUSION

Three-minute oscillations above a sunspot have been studied at both short (UV/EUV) and long (microwave) wavelengths. Intensity variations with $f = 5\text{--}9 \text{ mHz}$ are found in all analyzed UV/EUV bandpasses, as well as in microwaves (1.76 cm), with similar spectral characteristics. The largest modulation depth (20%) is found in the transition region (304 Å channel) and decreases down to the photosphere and up to the corona. Time delays between oscillations at different wavelengths above the umbra's center increase with the expected formation height of the corresponding emission (except for 211 Å). This confirms that observed intensity variations of both UV/EUV and microwave emission result from waves propagating upward. Measured delays are used to estimate average velocities of wave propagation at different layers of solar atmosphere and the altitude of microwave emission generation.

High spatial, temporal, and spectral resolution of SDO/AIA allowed us to trace the variations of the cutoff frequency and spectrum of oscillations across the umbra. We found that in the range 5–9 mHz high-frequency oscillations are more pronounced closer to the umbra's center, while the low frequencies concentrate on the peripheral parts. Accordingly, the cutoff frequency decreases from 5.7 to 5.0 mHz. We interpreted this discovery as a manifestation of variation of the magnetic field inclination across the umbra at the level of temperature minimum. This interpretation has been used for the diagnostics of sunspot atmospheres on this level.

Similar spectral characteristics of three-minute oscillations were found through all the temperature bandpasses. This suggests that the strong magnetic field of a sunspot works as a waveguide for the acoustic waves propagating from the photosphere level and eventually reaching a 1 MK corona.

The authors are grateful to Drs. M. Shimojo and W. R. Ashworth for useful discussions. We are thankful to an anonymous referee for suggesting improvements to an earlier version of this paper. The work was partly supported by RFBR grant nos. 10-02-00153, 11-02-91175, and 11-02-10000-k. The research carried out by Dr. Robert Sych at NAOC was supported by the Chinese Academy of Sciences Visiting Professorship for Senior International Scientists, grant no. 2010T2J24.

REFERENCES

- Abramov-Maximov, V. E., Gelfreikh, G. B., Kobanov, N. I., Shibasaki, K., & Chupin, S. A. 2011, *Sol. Phys.*, **270**, 175
- Avrett, E. H., & Loeser, R. 2008, *ApJS*, **175**, 229
- Bel, N., & Leroy, B. 1977, *A&A*, **55**, 239
- Bloomfield, D. S., Lagg, A., & Solanki, S. K. 2007, *ApJ*, **671**, 1005
- Bogdan, T. J., & Judge, P. G. 2006, *Philos. Trans. R. Soc. A*, **364**, 313
- Botha, G. J. J., Arber, T. D., Nakariakov, V. M., & Zhugzhda, Y. D. 2011, *ApJ*, **728**, 84
- Brynildsen, N., Maltby, P., Foley, C. R., Fredvik, T., & Kjeldseth-Moe, O. 2004, *Sol. Phys.*, **221**, 237
- Brynildsen, N., Maltby, P., Fredvik, T., & Kjeldseth-Moe, O. 2002, *Sol. Phys.*, **207**, 259
- Brynildsen, N., Maltby, P., Leifsen, T., Kjeldseth-Moe, O., & Wilhelm, K. 2000, *Sol. Phys.*, **191**, 129
- Centeno, R., Collados, M., & Trujillo Bueno, J. 2006, *ApJ*, **640**, 1153
- Centeno, R., Collados, M., & Trujillo Bueno, J. 2009, *ApJ*, **692**, 1211
- Christopoulou, E. B., Georgakilas, A. A., & Koutchmy, S. 2000, *A&A*, **354**, 305
- Christopoulou, E. B., Georgakilas, A. A., & Koutchmy, S. 2001, *A&A*, **375**, 617
- Christopoulou, E. B., Skodras, A., Georgakilas, A. A., & Koutchmy, S. 2003, *ApJ*, **591**, 416
- De Moortel, I. 2009, *Space Sci. Rev.*, **149**, 65
- De Moortel, I., Ireland, J., Hood, A. W., & Walsh, R. W. 2002, *A&A*, **387**, L13
- Felipe, T., Khomenko, E., & Collados, M. 2011, *ApJ*, **735**, 65
- Felipe, T., Khomenko, E., Collados, M., & Beck, C. 2010, *ApJ*, **722**, 131
- Fleck, B., & Schmitz, F. 1991, *A&A*, **250**, 235
- Gelfreikh, G. B., Grechnev, V., Kosugi, T., & Shibasaki, K. 1999, *Sol. Phys.*, **185**, 177
- Jain, R., & Haber, D. 2002, *A&A*, **387**, 1092
- Khomenko, E. V. 2009, in ASP Conf. Ser. 416, *Solar-Stellar Dynamos as Revealed by Helio- and Asteroseismology: GONG 2008/SOHO 21*, ed. M. Dikpati et al. (San Francisco, CA: ASP), 31
- Lamb, H. 1908, *Proc. London Math. Soc.*, Ser. 2, **7**, 122
- Maltby, P., Avrett, E. H., Carlsson, M., et al. 1986, *ApJ*, **306**, 284
- Marsh, M. S., & Walsh, R. W. J. 2006, *ApJ*, **643**, 540
- McIntosh, S., & Jefferies, S. 2006, *ApJ*, **647**, L77
- Nagashima, K., Sekii, T., Kosovichev, A. G., et al. 2007, *PASJ*, **59**, 631
- O'Dwyer, B., Del Zanna, G., Mason, H. E., Weber, M. A., & Tripathi, D. 2010, *A&A*, **521**, A21
- O'Shea, E., Muglach, K., & Fleck, B. 2002, *A&A*, **387**, 642
- Schwer, K., Lilly, R. B., Thompson, B. J., & Brewer, D. A. 2002, AGU Fall Meeting Abstracts, [abstract #SH21C-01](#)
- Shibasaki, K. 2001, *ApJ*, **550**, 1113
- Shibasaki, K., Enome, S., Nakajima, H., et al. 1994, *PASJ*, **46**, L17
- Solanki, S. K. 2003, *A&AR*, **11**, 153
- Sych, R., Nakariakov, V. M., Karlicky, M., & Anfinogentov, S. 2009, *A&A*, **505**, 791
- Sych, R., Zaqarashvili, T. V., Nakariakov, V. M., et al. 2011, *A&A*, in press (arXiv:1110.2556)
- Thomas, J. H., & Weiss, N. O. 2008, *Sunspots and Starspots* (Cambridge: Cambridge Univ. Press)
- Title, A. M., Hoeksema, J. T., Schrijver, C. J., & The Aia Team 2006, 36th COSPAR Scientific Assembly, **2600**
- Tziotziou, K., Tsiropoula, G., Mein, N., & Mein, P. 2006, *A&A*, **456**, 689
- Tziotziou, K., Tsiropoula, G., Mein, N., & Mein, P. 2007, *A&A*, **463**, 1153
- van der Voort, L. H. M. R., Rutten, R. J., Sütterlin, P., Sloover, P. J., & Krijger, J. M. 2003, *A&A*, **403**, 277
- Verwichte, E., Marsh, M., Foullon, C., et al. 2010, *ApJ*, **724**, L194
- Zheleznyakov, V. V. 1962, *SvA*, **6**, 3
- Zhugzhda, Y. D. 2008, *Sol. Phys.*, **251**, 501